Original Research

Endorectal Diffusion-Weighted Imaging in Prostate Cancer to Differentiate Malignant and Benign Peripheral Zone Tissue

Keyanoosh Hosseinzadeh, MD,* and Samuel David Schwarz, BA

Purpose: To determine if the apparent diffusion coefficient (ADC) can discriminate benign from malignant peripheral zone (PZ) tissue in patients with biopsy-proven prostate cancer that have undergone endorectal diffusion-weighted imaging (DWI) of the prostate.

Materials and Methods: Ten patients with prostate cancer underwent endorectal magnetic resonance imaging (MRI) in addition to DWI. A two-dimensional grid was placed over the axial images, and each voxel was graded by a 4-point rating scale to discriminate nonmalignant from malignant PZ tissue based on MR images alone. ADC was then determined for each voxel and plotted for nonmalignant and malignant voxels for the entire patient set. Second, with the radiologist aware of biopsy locations, any previously assigned voxel grade that was inconsistent with biopsy data was regrouped and ADCs were replotted.

Results: For the entire patient set, without and with knowledge of the biopsy data, the mean ADCs for nonmalignant and malignant tissue were 1.61 ± 0.27 and $1.34 \pm 0.38 \times 10^{-3}$ mm^2/second ($P = 0.002$) and 1.61 ± 0.26 and $1.27 \pm 0.37 \times 10^{-3}$ mm^2/second ($P = 0.0005$), respectively.

Conclusion: DWI of the prostate is possible with an endorectal coil. The mean ADC for malignant PZ tissue is less than nonmalignant tissue, although there is overlap in individual values.

Key Words: prostate cancer; endorectal magnetic resonance imaging; diffusion-weighted imaging; apparent diffusion coefficient; echo planar imaging; tumor
J. Magn. Reson. Imaging 2004;20:654–661.

PROSTATE CANCER IS THE MOST COMMON malignancy in males, and according to estimates made by the American Cancer Society, 230,110 new cases will be diagnosed and 29,900 deaths will occur in the year 2004 (1).

Currently, endorectal magnetic resonance imaging (MRI) in combination with a pelvic phased-array coil is the best available technique for tumor localization and staging in patients with prostate cancer (2–4). The combination of these coils allows high spatial-resolution images of the prostate gland to be obtained in addition to assessment of regional metastasis. The use of an endorectal coil for signal reception increases signal to noise by a factor of 10 over a pelvic phased-array coil (5). Endorectal MRI relies on signal abnormalities that result from morphologic changes within the prostate gland. However, the abnormal signal intensities do not accurately predict the volume (6–9) and extent of cancer in the gland (10), a fact confirmed by step-section histologic examination following en bloc radical prostatectomy. One reason for the lower sensitivity is the inconspicuous nature of the disease as manifested by subtle low-signal abnormalities, which preclude accurate contouring of the regions of suspected cancer involvement. Conventional MRI is also limited in specificity as other processes can mimic the low-signal-intensity changes associated with prostate cancer, notably postbiopsy hemorrhage, fibrosis, prostatitis, and prior therapy (2). Because of these limitations, new imaging modalities are being investigated to improve tumor localization and clinical staging.

One method currently being studied is diffusion-weighted imaging (DWI). DWI is sensitive to molecular translation of water in biologic tissues due to the random thermal motion of molecules. The microscopic motion includes molecular diffusion of water and microcirculation of blood in the capillary network, which represent incoherent motion. With the application of diffusion gradient pulses, MRI by means of the apparent diffusion coefficient (ADC) quantifies the combined effects of both diffusion and capillary perfusion. The random motion in the field gradients produces incoherent phase shifts, resulting in signal attenuation. The recent implementation of echo planar imaging (EPI) allows diffusion-weighted images to be obtained because of its short scanning time, and thus limits the effect of bulk motions. The primary application of DWI has been in brain imaging, mainly for the evaluation of acute ischemic stroke, demyelinating tumors, and intracra-

Department of Diagnostic Radiology, University of Maryland School of Medicine, Baltimore, Maryland.
Contract grant sponsor: NIH; Contract grant number: NHLB1-HL07612-16
Presented during Clinical Science Focus Session, International Society for Magnetic Resonance in Medicine, Toronto, Canada, 2003.
*Address reprint request to: K.H., Department of Diagnostic Radiology, University of Maryland School of Medicine, 22 S. Greene St., Baltimore, MD 21201. E-mail: khosseinzadeh@umm.edu
Received November 21, 2003; Accepted May 24, 2004.
DOI 10.1002/jmri.20159
Published online in Wiley InterScience (www.interscience.wiley.com).

Table 1
Grading of Voxels in Relation to Biopsy Results

Biopsy location	Patients	Cancer # voxels (%)	Benign # voxels (%)	Total # voxels
Unknown	10	142 (18)	645 (82)	787
Known	10	130 (17)	657 (83)	787

nial tumors (11). With the advent of faster imaging, DWI has been used to characterize abdominal organs and hepatic lesions (12–18), differentiate malignant and benign breast lesions (19), and evaluate small to medium cystic ovarian masses (20). The success that DWI has had clinically has led to a broadening of its application to the prostate gland. Gibbs et al (21) successfully investigated T2 relaxation rates and diffusion-weighted images of the human prostate using a pelvic phased-array coil. Mean ADCs for both malignant and normal peripheral zone (PZ) tissue were obtained. A recent study using a pelvic phased-array coil to image the prostate gland of patients with biopsy-proven cancer demonstrated significant differences in the ADCs between malignant PZ tissue and nonmalignant PZ tissue (22). The author concluded that prostate cancer can cause restricted diffusion of water relative to that of normal tissue, resulting in decreased signal of malignant lesions on ADC maps, and DWI may prove to be an effective adjunct tool in the localization and potential treatment of prostate cancer. Following a search of the literature from the National Library of Medicine (PubMed), no studies examining the correlation between measured ADCs obtained from DWI and endorectal MRI in patients with prostate cancer have been published.

Although prospective clinical observation of ADC maps demonstrates qualitatively decreased signal of malignant lesions in relation to benign tissue, the purpose of our preliminary study was to determine whether measured ADCs can differentiate cancer in the PZ from nonmalignant tissue using an endorectal coil in patients with biopsy-proven cancer. The possibility of a threshold value for ADC to distinguish nonmalignant from cancer tissue was also investigated.

MATERIALS AND METHODS

Conventional MRI

Between August 2000 and March 2001, 11 patients (mean age = 64 years, range = 51–78 years) with transrectal ultrasound (TRUS)-guided biopsy-confirmed prostate cancer were referred for combined endorectal/pelvic phased-array coil MRI for consideration of disease-targeted therapy. In this study, retrospective evaluation of the clinical and imaging data for these patients was approved by the Institutional Review Board. Routine systematic sextant TRUS biopsy (additional targeted biopsy was performed as necessary) was performed at least one month prior to imaging to minimize the effects of postbiopsy hemorrhage (23). Sextant biopsies were obtained from the basal, mid-, and apical parts of the prostate on each side. The body coil was used for signal excitation; the endorectal (Medrad, Pittsburgh, PA) and pelvic phased-array coils were used for signal reception of the prostate gland/seminal vesicles and coverage to the aortic bifurcation, respectively. One milligram of glucagon was administered intramuscularly before placement of the endorectal coil. The endorectal coil was insufflated with approximately 40 cc of air. All imaging was performed at 1.5 T (Philips Medical Systems, Eclipse (maximum gradient amplitude = 27 mT/m, maximum slew rate = 120 mT/m/second), Best, The Netherlands). For the endorectal component of the anatomical imaging, axial, coronal, and sagittal T2-weighted fast spin-echo (FSE) images (TR/TE = 3–4000/90 msec, ETL = 8, section thickness = 3 mm, matrix = 192 × 256, signal averages = 2) were performed through the prostate gland and seminal vesicles. Axial T1-weighted spin-echo (SE) images (TR/TE = 400/20 msec, section thickness = 3 mm, matrix = 192 × 256, signal averages = 2) were also obtained to evaluate for postbiopsy hemorrhage. The field of view (FOV) for all images was 20 × 20 cm. Surface coil correction was applied to all endorectal-acquired images. Finally, imaging through the pelvis to the aortic bifurcation was performed using a T2-weighted FSE sequence with frequency-selective fat suppression (TR/TE = 5–6000msec, ETL = 16, section thickness = 7 mm, matrix = 192 × 256, signal averages = 2). The total imaging time was approximately 20 minutes on average.

DWI

DWI was performed using single-shot EPI. A multislice single-shot diffusion-weighted EPI sequence was performed with two square diffusion gradient pulses applied before and after the 180° pulse (TR/TE = 10,000/99 msec, section thickness = 3 mm, matrix = 80 × 80, signal acquisition = 1, FOV = 20 × 20 cm) so

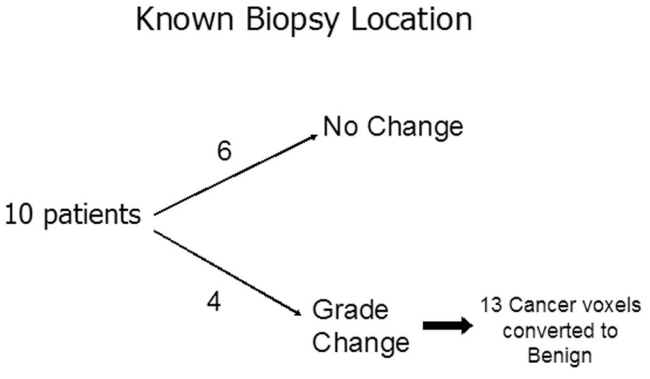

Figure 1. Changes in voxel grading with the radiologist aware of the biopsy location.

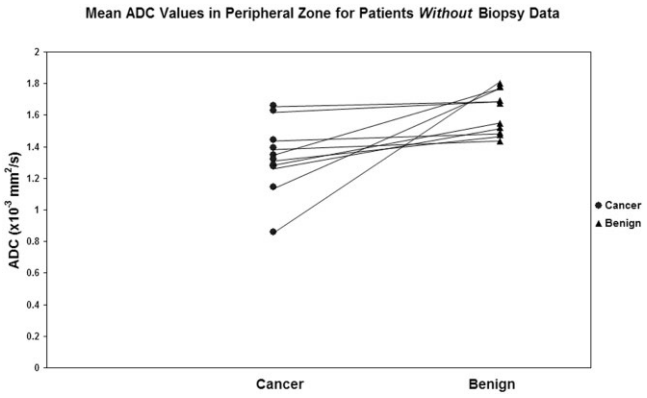

Figure 2. Chart demonstrates the mean ADCs of cancer and benign voxels for each patient. A line is drawn connecting the mean ADCs for each patient. For each patient, the mean ADC for malignant PZ is less than that for benign tissue.

as to coincide with the same slice locations as the axial T2-weighted FSE images using a diffusion sensitivity of b = 1000 seconds/mm^2. A high b-value was used to render the effects of the flow coefficient negligible. DWI was obtained by placing a frequency-selective radio frequency (RF) pulse before the pulse sequence to reduce chemical shift artifacts. The diffusion gradients were applied sequentially in three orthogonal axes to generate three sets of axial diffusion-weighted images. The total imaging time for DWI was one minute.

Image Analysis

Image analysis included T1- and T2-weighted images. The T1-weighted image was used for evaluation of post-biopsy hemorrhage and low-signal changes were recorded on the T2-weighted image. A rectangular grid was placed on the axial T2-weighted image, creating voxels of tissue that measure 7.5 × 7.5 × 3 mm (nine pixels), corresponding to a volume of 0.169 cc. Image analysis was divided into two parts. In the first experiment, voxels consisting of at least 75% PZ tissue were then graded on a 4-point rating scale (1 = definitely benign, 2 = probably benign, 3 = probably cancer, 4 = definitely cancer) by an experienced radiologist (K.H.) without knowledge of the biopsy data and location. The level of confidence in detecting cancer was based on conspicuity and shape of signal abnormalities involving the PZ on T2-weighted images. A rounded conspicuous low-signal lesion was considered cancer, whereas linear and triangular-shaped low-signal abnormalities were considered benign etiologies. For the purposes of statistical analysis, voxels with grades of 1 and 2 were classified as benign and voxels with grades of 3 and 4 were classified as cancer. In the second experiment, this analysis was repeated, allowing the radiologist to access the biopsy data. Any previously assigned voxel grade that was inconsistent with the biopsy data was regrouped as a benign or cancer voxel. Only those voxels located within a region of biopsy-confirmed cancer were grouped into the cancer voxels. For example, any voxel previously assigned a grade of 3 or 4, but found to be inconsistent with biopsy data, was regrouped as a benign voxel. Similarly, any voxel graded as benign but found to contain cancer on biopsy was regrouped as cancer.

ADCs were calculated in the PZ for all slices on a voxel-by-voxel basis by taking the average of the ADC computed from each of the three orthogonal-direction diffusion-weighted images. The ADC for each direction itself was computed according to the formula

$$ADC = [-\ln (S_1 - S_0)/(b_1 - b_0)]\ mm^2/s$$

where S_1 is the signal intensity of a voxel (nine pixels) after application of a diffusion gradient and S_o is the echo magnitude without diffusion gradients applied (b = 0 seconds/mm^2). Diffusion sensitivity is determined by the difference between b_1 and b_o, which in our case was 1000 seconds/mm^2.

Data Analysis

Quantitative analysis was also divided into two experiments. First, with the radiologist blinded to biopsy location, the ADCs for cancer and benign voxels were plotted for each patient individually and for the entire patient set.

Second, the ADCs for the revised cancer and benign voxels were plotted for each patient individually and for the entire patient set. An unpaired, one-tail *t*-test was performed assuming unequal variance between data for cancer and benign prostate in both experiments.

RESULTS

Of the 11 patients evaluated, 1 patient was excluded, as no reliable data were available documenting the location of cancer from the TRUS-guided biopsy. Therefore, in the initial experiment, with the radiologist blinded to biopsy location, 10 patients were studied, representing a total of 787 voxels. Of these, 142 (18%) voxels were grouped as cancer voxels (grade 3 = 121, grade 4 = 21), while 645 (82%) were classified as benign voxels (grade 1 = 74, grade 2 = 571). In the second experiment (Table 1), with the radiologist able to access the biopsy location data, 10 patients were studied, representing a total of 787 voxels. Of these, 130 (17%) were grouped as cancer voxels (grade 3 = 118, grade 4 = 12), while 657 (83%) were classified as benign voxels (grade 1 = 72, grade 2 = 585). Six of 10 patients had no change in data since the images were graded appropriately. In the remaining four patients, a total of only 13 cancer voxels were reclassified as benign, while no benign voxels were reclassified as cancer (Fig. 1).

Without knowledge of biopsy location, the mean ADCs averaged for the entire patient set for benign and cancer voxels were 1.61 ± 0.27 and 1.34 ± 0.38 × 10^{-3} mm^2/second, respectively (P = 0.002). With knowledge of biopsy locations, the mean ADCs averaged over 10 patients for benign and cancer voxels were 1.61 ± 0.26 and 1.27 ± 0.37 × 10^{-3} mm^2/second, respectively (P = 0.0005). In both experiments, the mean ADCs were lower for malignant PZ tissue than for nonmalignant PZ tissue. Second, the mean ADC for malignant tissue decreased slightly when the reader was allowed access

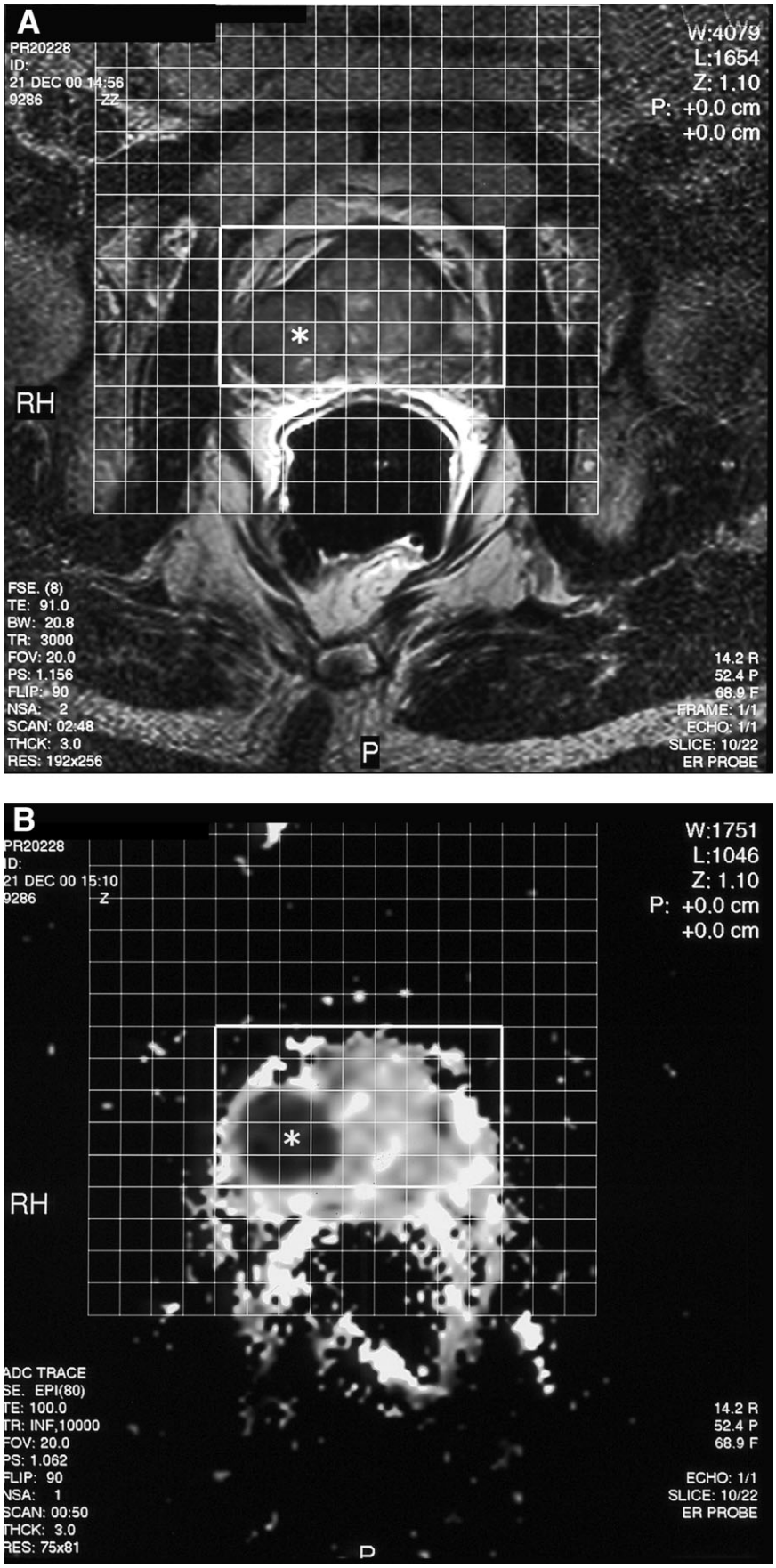

Figure 3. (continued)

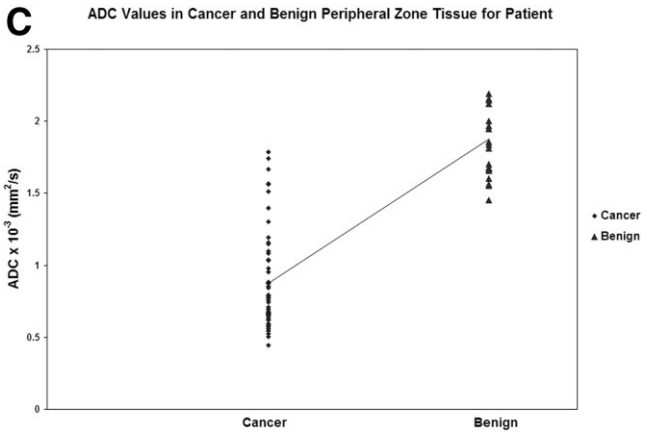

Figure 3. A: Axial T2-weighted image of the prostate with a rectangular grid demonstrating the presence of a large tumor in the right PZ (asterisk). **B:** Axial ADC trace of the prostate with a rectangular grid demonstrating large low-signal tumor (asterisk). **C:** Chart illustrating ADCs for all cancer and benign voxels for patient. Mean ADC for cancer voxels is significantly less than that for benign voxels, although overlap exists in individual values.

to the biopsy data. The change is partially related to the regrouping of 13 cancer voxels to benign. Although significant differences exist in the mean ADCs, large overlap was noted in the individual values in both tissue types (Fig. 2). In addition to the mean ADCs for the entire patient set, the mean ADC was greater in benign voxels than in cancer voxels for the individual patients for both experiments. Diffusion-weighted images can demonstrate malignant PZ tissue with clarity, although variable signal range was present in the patient population. In a patient with biopsy-proven cancer in the right PZ (Fig. 3), the mean ADC for cancer voxels was $0.86 \pm 0.33 \times 10^{-3}$ mm^2/second, while the mean ADC for the benign voxels was $1.80 \pm 0.22 \times 10^{-3}$ mm^2/second. The difference between the patient's mean ADCs is not only statistically significant, but it is larger than the difference between the mean ADCs for the entire patient set. In this patient, knowledge of the biopsy location caused no change in the patient data as the MR images were graded appropriately. ADCs can also be helpful in discriminating postbiopsy hemorrhage from malignant PZ tissue, as hemorrhage can mimic cancer on FSE T2-weighted images (Fig. 4). Hemorrhage can delineate tumor on T1-weighted images because the densely cellular tumor is outlined by impenetrable blood, as the presence and diffuse spread of hemorrhage can be attributed to the ductal morphology of the prostate gland (23).

DISCUSSION

DWI of the human prostate has been successfully demonstrated using an endorectal coil. It is well known that increased signal to noise is obtained when an endorectal coil is used for signal reception, and yields images of high spatial-resolution. The potential for susceptibility artifact from air insufflation during EPI did not degrade the diagnostic quality of the ADC maps, and no geometric distortion was detected. While fluid insufflation poses certain theoretical advantages, this option is not commercially available to our knowledge. As previously mentioned, a high b-value was chosen to enable the signal intensity dependent on the diffusion term. Lower b-values with the use of a pelvic phased-array coil in evaluating the prostate gland (22) have been investigated, although an optimal b-value has not been determined. A lower range of b-values may be necessary given the reduced signal to noise from use of a pelvic phased-array coil. However, unlike the abdomen, where a high b-value can diminish image quality because of short T2 time of abdominal tissues (13), nonmalignant/normal PZ tissue has high T2 values, as opposed to the short T2 time of prostate cancer (24). Consequently, lesion contrast and image quality can be maintained during EPI acquisition, together with accurate measurement of ADC, with the use of an endorectal coil. Further studies are currently in progress to optimize b-values with use of an endorectal coil, such that lesion contrast and signal are optimized within a background of high-signal PZ.

Optimal evaluation of patients with prostate cancer necessitates the use of both a pelvic phased-array coil and an endorectal coil with current field strengths in clinical practice. The results in our study demonstrate that there is a statistically significant difference between mean ADCs for cancer and nonmalignant PZ tissue whether or not the reader was aware of the biopsy sites of tumor burden. The difference may be explained by certain anatomical changes caused by the replacement of normal tissue with cancer. The normal prostate consists of a glandular component and intervening stromal tissue. The glandular component of the prostate gland consists of water-rich ducts arranged in a linear fashion radiating from the prostatic urethra, which terminate into acini. In prostate cancer, the normal architecture of the gland is replaced by adenocarcinoma. The tumor can contain high densities of malignant epithelial cells and a reduction in intervening stroma; however, in others, malignant epithelial cells can be dispersed between increased amounts of desmoplasmic stroma as well as between normal-appearing ductal morphology, as in early diffuse disease (22,25). All three of these morphologic conditions inhibit the movement of water macromolecules by the internal derangement introduced by the regions of tumor burden, and may account for the variations of the ADCs, as well as overlap between ADCs for regions of cancer and those of nonmalignant PZ tissue. Therefore, at this point in time, a quantitative ADC threshold value does not permit discrimination of malignant PZ from nonmalignant tissue. Rather, analysis of patient data requires consideration of the available clinical history, including TRUS biopsy information, digital rectal examination (DRE) findings, prostate specific antigen (PSA), and MRI. The incorporation of DWI into the prostate imaging protocol at our institution provides useful information in conjunction with conventional anatomic MRI. Currently, however, the ADC maps are evaluated qualitatively with the corresponding anatomic images. In a recent publication using a pelvic phased-array coil for signal reception, similar findings were reported, al-

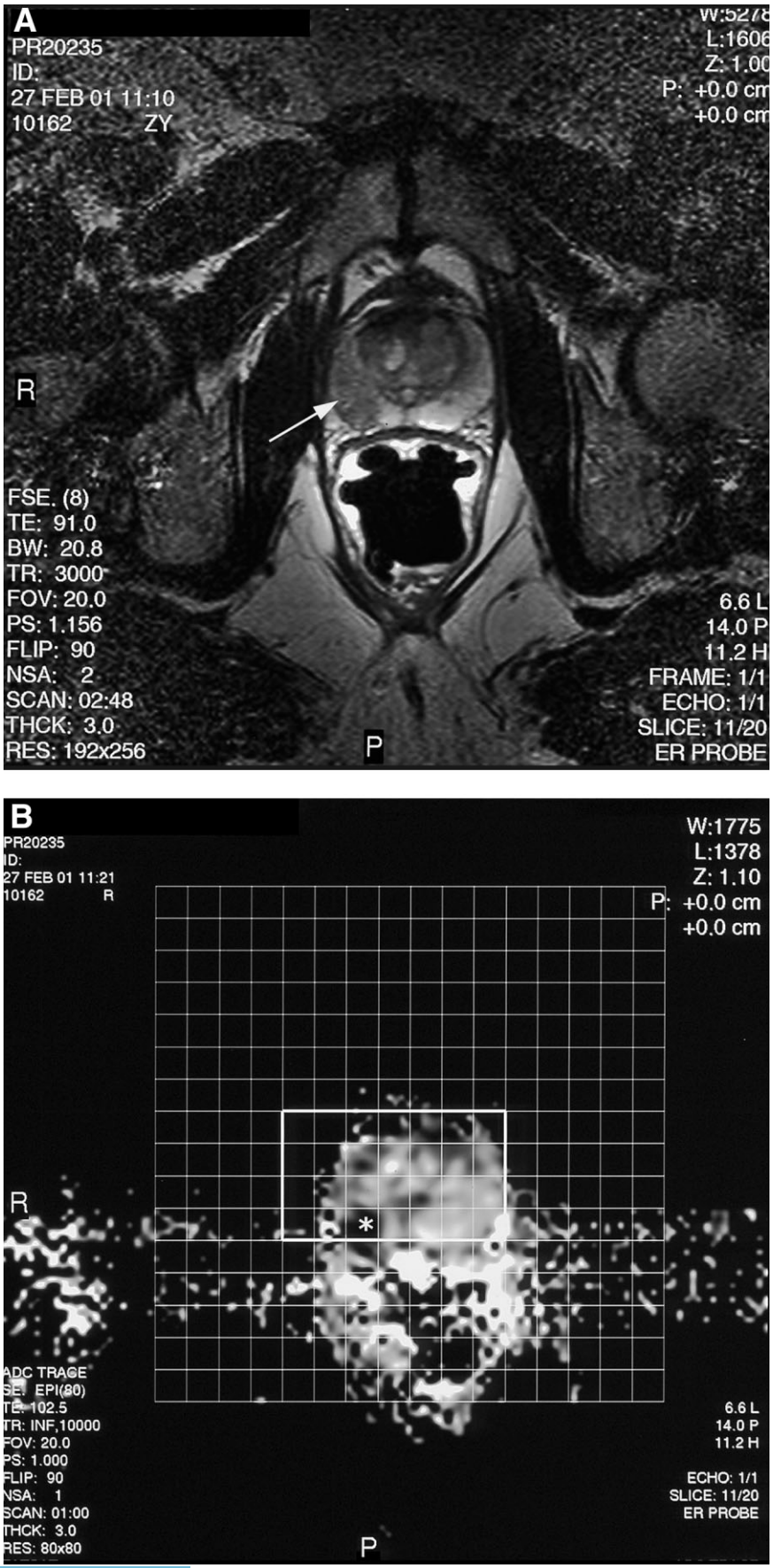

Figure 4. **A:** Axial T2-weighted image of the prostate demonstrating a large region of low signal in the right PZ (arrow). **B:** Axial ADC trace of the prostate with a rectangular grid demonstrates smaller low-signal lesion (asterisk). **C:** Axial T1-weighted image of the prostate demonstrating the presence of postbiopsy hemorrhage delineating the area of tumor (arrow) in the right PZ.

Figure 4 (Continued)

though signal to noise and resolution limitations compromised image quality (22). In our study, slice thickness was kept at 3 mm, covering the entire gland from the base to the apex. A further advantage of the endorectal coil is decreased imaging time, as fewer acquisitions are required to obtain high-quality images free of motion artifacts.

The PZ of the prostate was examined exclusively for several reasons. It is known that 70% of all adenocarcinomas of the prostate arise in the PZ and 30% in the central gland (26). Furthermore, benign prostatic hyperplasia (BPH) of the central gland occurs in 25% of men from 41–50 years and 70% of men from 61–70 years (27). BPH manifests in a variety of histological forms, depending on the amount of glandular and stromal tissue, and the signal characteristics in MRI reflect the morphological differences. Cancer can occur in the central gland, and in such cases, MRI cannot reliably distinguish BPH from cancer, as opposed to cancer within the PZ. This is because changes in MRI signal intensity that commonly occur in older patients with BPH are similar to those that occur in patients with prostate cancer (25,28–31). Furthermore, quantitative T2 mapping and DWI of the prostate central gland have failed to show statistical difference in T2 and mean ADCs between BPH and prostatic carcinoma (21). The authors concluded that morphological changes of BPH subsequently cause changes in the tissue structure that can affect the properties of water diffusion. These structural changes can lead to inaccurate ADC measurements of the central gland and false positive results on a DWI sequence.

A single radiologist experienced in MRI of the prostate reviewed the anatomical imaging, which precluded assessment of interobserver variability for multiple readers. The authors acknowledge the direct relationship of improved staging accuracy of MRI of the prostate with reader experience, which is an important application for this study design, as a reader with less experience may provide a different grading system. The majority of voxels were graded as "probably benign" or "probably malignant," and a small fraction as "definitely benign" and "definitely malignant." However, the purpose of our study was not to assess reader variability for conventional anatomic images, but to determine if the ADCs gained from DWI correlated with accurately interpreted endorectal MR images, which would require an experienced reader. This study is limited by the relatively small number of patients and the incomplete spatial assignment of the MRI findings to the biopsy sites. Ideally, imaging findings should be correlated to histopathologic sectioning where the prostate gland is removed en bloc and sections are matched in thickness with the images. With this technique it would be theoretically possible to match MRI and DWI findings with the histopathologic findings on a voxel-by-voxel basis. The patients in our study were being considered for disease-targeted therapy and did not undergo prostatectomy. Regions of interest cannot be accurately created for MRI and DWI independent of one another because DWI is not a high-resolution anatomical imaging technique, and tumor burden does not always appear as a conspicuous abnormality to allow margins of interest to be reliably drawn. The use of voxels would

allow overlap of imaging data in a future study with metabolite maps obtained from MR spectroscopic imaging of the prostate.

This study represents some of the first steps toward harnessing the potential impact of endorectal-acquired DWI as it relates to prostate cancer. Improvements in gradient field strengths, multishot techniques, and the introduction of parallel imaging techniques would be helpful in maximizing spatial resolution, and decreasing susceptibility-induced artifacts. Additional work with DWI in the field of prostate cancer diagnosis and treatment may lead to an improvement of tissue sampling in biopsies of the prostate gland as well as an improvement in the efficiency of disease-targeted therapies.

REFERENCES

1. American Cancer Society. Available at http://www.cancer.org/downloads/STT/CAFF_finalPWSecured.pdf.
2. Kurhanewicz J, Vigneron DB, Males RG, Swanson MG, Yu KK, Hricak H. The prostate: MR imaging and spectroscopy. Present and future. Radiol Clin North Am 2000;38:115–138.
3. Yu KK, Hricak H, Alagappan R, Chernoff DM, Bacchetti P, Zaloudek CJ. Detection of extracapsular extension of prostate carcinoma with endorectal and phased-array coil MR imaging: multivariate feature analysis. Radiology 1997;202:697–702.
4. Schnall MD, Imai Y, Tomaszewski J, Pollack HM, Lenkinski RE, Kressel HY. Prostate cancer: local staging with endorectal surface coil MR imaging. Radiology 1991;178:797–802.
5. Kurhanewicz J, Swanson MG, Nelson SJ, Vigneron DB. Combined magnetic resonance imaging and spectroscopic imaging approach to molecular imaging of prostate cancer. J Magn Reson Imaging 2002;16:451–463.
6. Kahn T, Burrig K, Schmitz-Drager B, Lewin JS, Furst G, Modder U. Prostatic carcinoma and benign prostatic hyperplasia: MR imaging with histopathologic correlation. Radiology 1989;173:847–851.
7. Sommer FG, Nghiem HV, Herfkens R, McNeal J, Low RN. Determining the volume of prostatic carcinoma: value of MR imaging with an external-array coil. AJR Am J Roentgenol 1993;161:81–86.
8. Jager GJ, Ruijter ET, van de Kaa CA, et al. Local staging of prostate cancer with endorectal MR imaging: correlation with histopathology. AJR Am J Roentgenol 1996;166:845–852.
9. Coakley FV, Kurhanewicz J, Lu Y, et al. Prostate cancer tumor volume: measurement with endorectal MR and MR spectroscopic imaging. Radiology 2002;223:91–97.
10. Yu KK, Hricak H. Imaging prostate cancer. Radiol Clin North Am 2000;38:59–85.
11. Geijer B, Holtas S. Diffusion-weighted imaging of brain metastases: their potential to be misinterpreted as focal ischaemic lesions. Neuroradiology 2002;44:568–573.
12. Chan JH, Tsui EY, Luk SH, et al. Diffusion-weighted MR imaging of the liver: distinguishing hepatic abscess from cystic or necrotic tumor. Abdom Imaging 2001;26:161–165.
13. Ichikawa T, Haradome H, Hachiya J, Nitatori T, Araki T. Diffusion-weighted MR imaging with single-shot echo-planar imaging in the upper abdomen: preliminary clinical experience in 61 patients. Abdom Imaging 1999;24:456–461.
14. Laghi A, Catalano C, Assael FG, et al. [Diffusion-weighted echo-planar sequences for the evaluation of the upper abdomen: technique optimization] [In Italian]. Radiol Med 2001;101:213–218.
15. Moteki T, Horikoshi H, Oya N, Aoki J, Endo K. Evaluation of hepatic lesions and hepatic parenchyma using diffusion-weighted reordered turboFLASH magnetic resonance images. J Magn Reson Imaging 2002;15:564–572.
16. Namimoto T, Yamashita Y, Mitsuzaki K, Nakayama Y, Tang Y, Takahashi M. Measurement of the apparent diffusion coefficient in diffuse renal disease by diffusion-weighted echo-planar MR imaging. J Magn Reson Imaging 1999;9:832–837.
17. Ries M, Jones RA, Basseau F, Moonen CT, Grenier N. Diffusion tensor MRI of the human kidney. J Magn Reson Imaging 2001;14:42–49.
18. Taouli B, Vilgrain V, Dumont E, Daire JL, Fan B, Menu Y. Evaluation of liver diffusion isotropy and characterization of focal hepatic lesions with two single-shot echo-planar MR imaging sequences: prospective study in 66 patients. Radiology 2003;226:71–78.
19. Guo Y, Cai YQ, Cai ZL, et al. Differentiation of clinically benign and malignant breast lesions using diffusion-weighted imaging. J Magn Reson Imaging 2002;16:172–178.
20. Moteki T, Ishizaka H. Diffusion-weighted EPI of cystic ovarian lesions: evaluation of cystic contents using apparent diffusion coefficients. J Magn Reson Imaging 2000;12:1014–1019.
21. Gibbs P, Tozer DJ, Liney GP, Turnbull LW. Comparison of quantitative T2 mapping and diffusion-weighted imaging in the normal and pathologic prostate. Magn Reson Med 2001;46:1054–1058.
22. Bashar I. In vivo measurement of the apparent diffusion coefficient in normal and malignant prostatic tissues using echo-planar imaging. J Magn Reson Imaging 2002;16:196–200.
23. White S, Hricak H, Forstner R, et al. Prostate cancer: effect of postbiopsy hemorrhage on interpretation of MR images. Radiology 1995;195:385–390.
24. Liney GP, Lowry M, Turnbull LW, et al. Proton MR T2 maps correlate with the citrate concentration in the prostate. NMR Biomed 1996;9:59–64.
25. Schiebler ML, Tomaszewski JE, Bezzi M, et al. Prostatic carcinoma and benign prostatic hyperplasia: correlation of high-resolution MR and histopathologic findings. Radiology 1989;172:131–137.
26. McNeal JE. Normal anatomy of the prostate and changes in benign prostatic hypertrophy and carcinoma. Semin Ultrasound CT MR 1988;9:329–334.
27. Grossfeld GD, Coakley FV. Benign prostatic hyperplasia: clinical overview and value of diagnostic imaging. Radiol Clin North Am 2000;38:31–47.
28. Bryan PJ, Butler HE, Nelson AD, et al. Magnetic resonance imaging of the prostate. AJR Am J Roentgenol 1986;146:543–548.
29. Ling D, Lee JK, Heiken JP, Balfe DM, Glazer HS, McClennan BL. Prostatic carcinoma and benign prostatic hyperplasia: inability of MR imaging to distinguish between the two diseases. Radiology 1986;158:103–107.
30. Poon PY, McCallum RW, Henkelman MM, et al. Magnetic resonance imaging of the prostate. Radiology 1985;154:143–149.
31. Schnall MD, Lenkinski RE, Pollack HM, Imai Y, Kressel HY. Prostate: MR imaging with an endorectal surface coil. Radiology 1989;172:570–574.